

# Extraction and Analysis of the Characteristic Parameters in Back-to-Back Connected Asymmetric Schottky Diode

Zuo Wang, Wanyu Zang, Yeming Shi, Xingyu Zhu, Gaofeng Rao, Yang Wang, Junwei Chu, Chuanhui Gong, Xiuying Gao, Hui Sun, Sibao Huanglong, Dingyu Yang, and Peihua Wangyang\*

The physical Schottky parameters of devices based on Schottky contact are important to analyze the working mechanism. This article theoretically studies the parameter characteristics of the current–voltage curve of two back-to-back connected Schottky contacts via the thermionic emission model, and it is found that not all the parameters are able to be extracted under some constraints. Compared with some classical extraction methods, a straightforward strategy to approach the Schottky intrinsic parameters by solving equations during the characteristic interval are presented. In addition, this method is verified on several representative standard curves and experimental curves, and the extracted parameters are highly compatible with those curves. The current extraction method will be of great significance for the design and preparation of Schottky-based devices.

## 1. Introduction

Metal–semiconductor (MS) contacts are widely used in modern electronic devices.<sup>[1–7]</sup> Current MS contacts could be generally classified into Ohmic contacts and Schottky contacts. In the ohmic contacts, there is no voltage drop through the MS interface, which results in a symmetrical current–voltage curve obeying Ohm's law. And in the Schottky contacts, there is a so-called space charge region on the semiconductor side, and a potential barrier forms consequently.<sup>[1]</sup> This barrier causes rectifying behavior, and its diodes can be built into high-frequency rectification, while reducing energy consumption and electronic noise, improving work efficiency and frequency.<sup>[8,9]</sup> In the applications, ideality factors, barrier heights, and series resistance are

important for designing and manufacturing the electronic devices.<sup>[5]</sup> Therefore, it is necessary to acquire the characteristic parameters of the Schottky diode. Fortunately, on the basis of thermionic emission theory, the current–voltage curve contains enough characteristics that can be effectively used in parameters extraction.<sup>[10–12]</sup>


There are many strategies put forward to extract parameters of MS diode impacted by a single Schottky barrier height.<sup>[13–29]</sup> In these articles, the Bennett method is convenient and practical. All it needs is to select a certain range of forward bias to solve a system of linear equations.<sup>[21]</sup> In recent years, nevertheless, parameter extraction techniques based on artificial intelligence using all kinds of algorithms

have been developed, such as genetic algorithm, simulated annealing algorithm, and differential evolution method, providing us a more accurate fitting scheme.<sup>[7,30–35]</sup> In addition, some methods for parameter extraction in back-to-back connected Schottky contacts were also developed in the last few years.<sup>[36–39]</sup> Nouchi found the identical region between MS contact and metal–semiconductor–metal (MSM) contact.<sup>[39]</sup> And in this identical region, an MSM diode can be regarded as an MS diode. Thus, there is only one group characteristic of single Schottky barrier parameters in the identical region. So, it is relatively simpler to extract those parameters of a single Schottky barrier first and then extrapolate another Schottky barrier. But this method is inoperative when two barrier heights are too close to make the identical region invisible.

To the best of our knowledge, series resistance has not got enough attention in MSM contact. Moreover, there is still not enough research on the characteristic of all parameters in back-to-back connected Schottky contacts as well as the analysis of parameter validity. Based on thermionic emission theory, in this article, the impact of ideal MSM contact parameters on the current–voltage curve in several certain conditions is analyzed. In addition, according to the characteristic interval, a method to approximate those parameters is proposed via solving equations. The results of our method are compared with those of the Bennett method and we find it is highly compatible with the experimental results. Our works provide a new and reliable solution for the parameter extraction of back-to-back connected Schottky contacts in the future.

Z. Wang, W. Zang, Y. Shi, X. Zhu, Dr. X. Gao, Dr. H. Sun, S. Huanglong, Prof. D. Yang, Dr. P. Wangyang  
College of Optoelectronic Technology  
Chengdu University of Information Technology  
Chengdu 610054, China  
E-mail: wangyph@cuit.edu.cn

Dr. G. Rao, Dr. Y. Wang, Dr. J. Chu, Dr. C. Gong, Dr. P. Wangyang  
Electronic Thin Film and Integrated Devices  
University of Electronic Science and Technology of China  
Chengdu 610054, China  
E-mail: wangyangpeihua@hotmail.com

 The ORCID identification number(s) for the author(s) of this article can be found under <https://doi.org/10.1002/pssa.201901018>.

DOI: 10.1002/pssa.201901018

## 2. Theory

When the Schottky barrier width is much smaller than the mean free path of an electron, the current transfer through the interface is usually described by the thermionic emission.<sup>[40]</sup> The expression for the current is<sup>[41]</sup>

$$I = I_0 \left[ \exp\left(\frac{\beta V}{n}\right) - 1 \right] \quad (1)$$

with  $\beta = \frac{q}{kT}$

$$I_0 = AA^{**} T^2 \exp(-\beta \phi_b) \quad (2)$$

and  $A^{**} = \frac{4\pi q m^* k^2}{h^3}$

where  $I_0$  is the saturation current,  $\beta$  is the inverse thermal voltage,  $V$  is the potential drop,  $q$  is the unit electronic charge,  $k$  is the Boltzmann constant,  $T$  is the absolute temperature,  $A$  is the contact area,  $\phi_b$  is the Schottky barrier height in volts,  $m^*$  is the effective mass of the charge carrier,  $h$  is the Planck constant,  $A^{**}$  is the effective Richardson constant, and  $n$  is called the ideality factor. For thermionic emission, the ideality factor is equal to 1, and when other emission mechanisms such as field-enhanced tunneling and thermally assisted tunneling work on current transport, this parameter is larger than 1.<sup>[39]</sup>

Actually, as shown in Figure 1, the back-to-back connected asymmetric Schottky diodes are commonly used in electronic devices.<sup>[42]</sup> In this case, one current flows through two back-to-back connected diodes with a series resistance and two voltage drops polarized in the opposite direction. According to Equation (1), the voltage drop on the back-to-back connected Schottky diodes is their sum on two interfaces and on series resistance<sup>[41]</sup>

$$V = V_1 + V_2 + RI = \frac{n_1}{\beta} \ln\left(\frac{I}{I_{01}} + 1\right) - \frac{n_2}{\beta} \ln\left(-\frac{I}{I_{02}} + 1\right) + RI \quad (3)$$

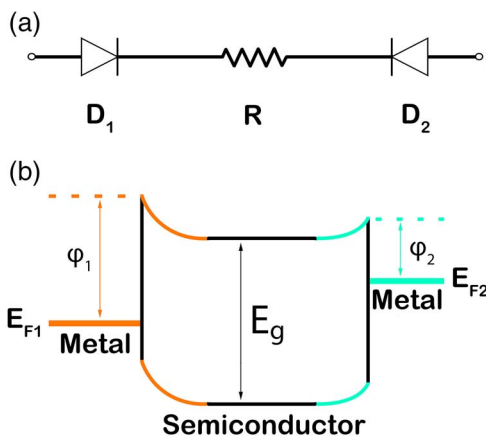


**Figure 1.** a) Two Schottky barriers connected back to back with series resistance. b) The energy band diagram of MSM contact with different barrier heights and n-type semiconductor under equilibrium, and with external bias applied.

where  $R$  is the series resistance,  $V_1$  and  $V_2$  are the voltage drops on the forward and reverse polarized diodes,  $n_1$  and  $n_2$  are two different ideality factors of the two opposite diodes, and  $I_{01}$  and  $I_{02}$  are two saturation currents of the two diodes, respectively.

## 3. General Investigation of Current–Voltage Curve

Standard representative current–voltage curves of back-to-back connected Schottky diodes with various combinations of parameters are generated from Equation (3), as shown in Figure 2. From Figure 2a–d, one can see that  $I_{02}$  goes down as  $\phi_2$  increases. It is interesting to find that the  $\phi_2$  becomes indistinguishable, thus making the current–voltage curves overlapped in a detectable coordinate scale, as the inset in Figure 2a–d shows. However, indistinguishable curves of Figure 2a–d will eventually become recognizable when a voltage is applied that is large enough in theory (the figure is not shown here). To figure out how the ideality factors and series resistance impact on Equation (3), four barrier heights conditions 1)  $\phi_1 = 0.8$  V,  $\phi_2 = 0.75$  V, 2)  $\phi_1 = 0.4$  V,  $\phi_2 = 0.35$  V, 3)  $\phi_1 = 0.8$  V,  $\phi_2 = 0.4$  V, and 4)  $\phi_1 = 0.3, 0.6, 0.9$  V,  $\phi_2 = 0$  V are generalized. Those barrier heights are combined with ideality factors (Figure 2e–h) and series resistance (Figure 2i–l), respectively. In Figure 2e, two ideality factors  $n_1$  and  $n_2$  can be well distinguished from the curve of two large barriers. And it is worth noting that ideality factor  $n_1$  is easier to distinguish than  $n_2$ . On the contrary, we can see that in two smaller barriers such as in Figure 2f, neither ideality factor  $n_1$  or  $n_2$  can be distinguished, which makes the extraction of two ideality factors impossible. After that, in Figure 2g, the barrier  $\phi_1$  is large and  $\phi_2$  is small. One can find that the ideality factors  $n_2$  cannot be effectively identified, which is similar to Figure 2f. And  $n_1$  in Figure 2g can be easily identified. Furthermore, in Figure 2h, we fixed the barrier  $\phi_2$  to 0 and changed  $\phi_1$  and  $n_1$  at the same time. It can be seen that the larger  $\phi_1$  is, the easier it is to distinguish  $n_1$ . According to Figure 2e–h, the ideality factor of one Schottky diode becomes distinguishable only if the barrier height of this Schottky diode is big enough. Finally, the impact of the series resistance  $R$  is also analyzed in Figure 2i–l. In Figure 2i, the two barriers are so large that the resistance can only be distinguished by an order of magnitude greater than 1 000 000. In Figure 2j, the two barriers are small, which allows the resistance to be distinguished on the magnitude of several Ohms. Similarly, resistors in Figure 2k,l can also be distinguished by several Ohms. Therefore, according to Figure 2i–l the influence of series resistance can be seen on current–voltage curves only in the case when the series resistance is so high that it drives the current–voltage curves already in reverse direction of the studied diodes, either the first diode or the second one.

In general, the characteristics of parameters can be quickly understood by comparing the experimental current–voltage curve with Figure 2 during the practical analysis. In addition, based on the previous discussion, some parameters can be effectively extracted from the experimental curve, whereas others cannot due to the barrier condition or actual voltage limitation.

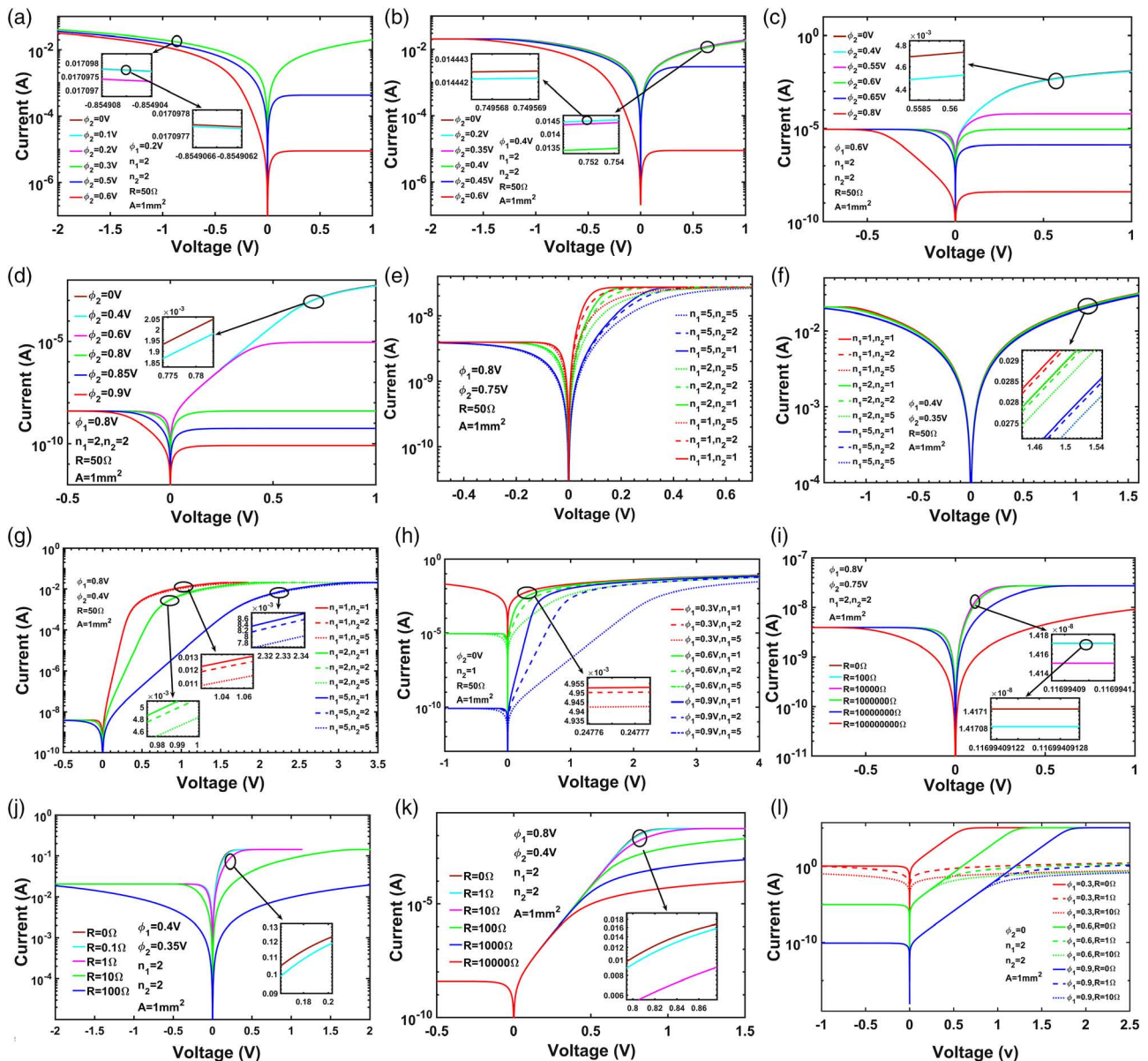


**Figure 2.** Current–voltage curves of back-to-back connected asymmetric Schottky diodes in various conditions of barrier heights, ideality factors and series resistance. The barrier height  $\phi_2$  varied and  $\phi_1$  was fixed as a) 0.2, b) 0.4, c) 0.6, and d) 0.8 V, respectively. Various combinations of ideality factors with e)  $\phi_1 = 0.8$  V,  $\phi_2 = 0.75$  V, f)  $\phi_1 = 0.4$  V,  $\phi_2 = 0.35$  V, and g)  $\phi_1 = 0.8$  V,  $\phi_2 = 0.4$  V. h) Various ideality factors  $n_1$  and  $\phi_1$  with fixed  $\phi_2 = 0$  V. Various series resistances  $R$  with i)  $\phi_1 = 0.8$  V,  $\phi_2 = 0.75$  V, j)  $\phi_1 = 0.4$  V,  $\phi_2 = 0.35$  V, and k)  $\phi_1 = 0.8$  V,  $\phi_2 = 0.4$  V. l) Various series resistances  $R$  and  $\phi_1$  with fixed  $\phi_2 = 0$  V.

Moreover, here we also propose two experiences to support the following parameter extraction scheme. It can be clearly seen from Figure 2g that the ideality factor  $n_1$  determines the slope of the linear part of the curve under logarithmic coordinates, and Figure 2k implies that the series resistance  $R$  determines when the linear part bends down to form an exponential curve.

Furthermore, actual electronic devices are greatly affected by temperature, so the influences of temperature on the current–voltage curve are also analyzed. It can be seen from Equation (2) that both the temperature and the Richardson constant can

directly affect saturation currents. And from Equation (3), temperature and saturation currents directly contribute to the current–voltage curve. To simplify the effect of temperature on the current–voltage curve during calculation, we suppose that the effective Richardson constant stays the same as temperature varies over a certain range. A comparison of different temperatures at three different barriers conditions is shown in Figure 3. One can see that saturation currents in two directions go up as temperature increases and the slope of the linear part is gradually changed with temperature.

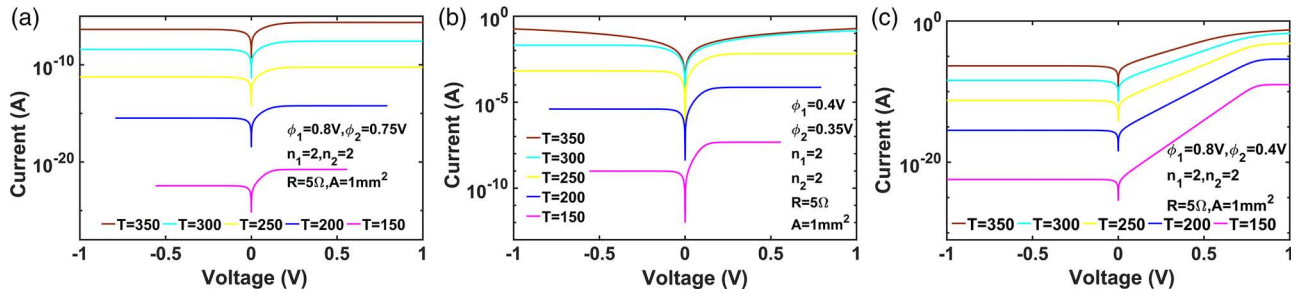


**Figure 3.** Current-voltage curve changes with several temperatures in three different barrier conditions: a)  $\phi_1 = 0.8$  V,  $\phi_2 = 0.75$  V, b)  $\phi_1 = 0.4$  V,  $\phi_2 = 0.35$  V, and c)  $\phi_1 = 0.8$  V,  $\phi_2 = 0.4$  V, respectively.

#### 4. The Proposed Method

To understand Equation (3) better, it can be rewritten as

$$\frac{dV}{dI} = SR(I) + R \quad (4)$$

$$\text{with } SR(I) = \frac{n_1}{\beta(I_{01}+I)} + \frac{n_2}{\beta(I_{02}-I)}$$

where the function  $SR(I)$  is named SR (Schottky-related resistance, SR) function, which represents the resistance caused by two Schottky contact interfaces for the external resistance. Figure 4a–d shows the SR function of different combinations of barrier heights with different ideality factors; the horizontal current ranges from  $I_{01}$  to  $I_{02}$ . One can see that  $n_1$  and  $n_2$  becomes discernible when the current gets close to  $I_{01}$  and  $I_{02}$ , as shown in Figure 4a–d, respectively.

Figure 4a shows when the current approaches two saturated currents  $I_{01}$  and  $I_{02}$ , the SR tends to infinity, and the slope of the current-voltage curve tends to zero (as shown in Figure 2 and 3). Hence, theoretically the current corresponding to the curve slope

of zero under positive and negative bias is the saturation current. In fact, the saturation current under reverse bias might be hidden by the image force and the tunneling effect.<sup>[40]</sup> It is reported that the measured current under bias of  $-0.1$  V is 96% of the saturation current in the case of a nearly ideal single diode.<sup>[43]</sup> Usually it is difficult to determine the saturation current directly on the forward bias curve, but when  $I_{02}$  is much larger than  $I_{01}$  and  $n_1$  is close to  $n_2$ , twice the maximum slope current is the most likely saturation current. (See the extrapolates saturation current under forward bias in the Supporting Information.)

After obtaining saturation currents, the remaining parameters in the equation are the ideality factors  $n_1$ ,  $n_2$  and series resistance  $R$ . In view of these three parameters, the equation is simplified into a linear equation. Theoretically, the parameters  $n_1$ ,  $n_2$ , and  $R$  can be solved by constructing a system of simultaneous equations of three points on the current-voltage curve. However, in practical calculation, it might produce a great error by arbitrarily choosing three points to solve the equations. Hence, it is vital to find the characteristic interval of each parameter to reduce the error.

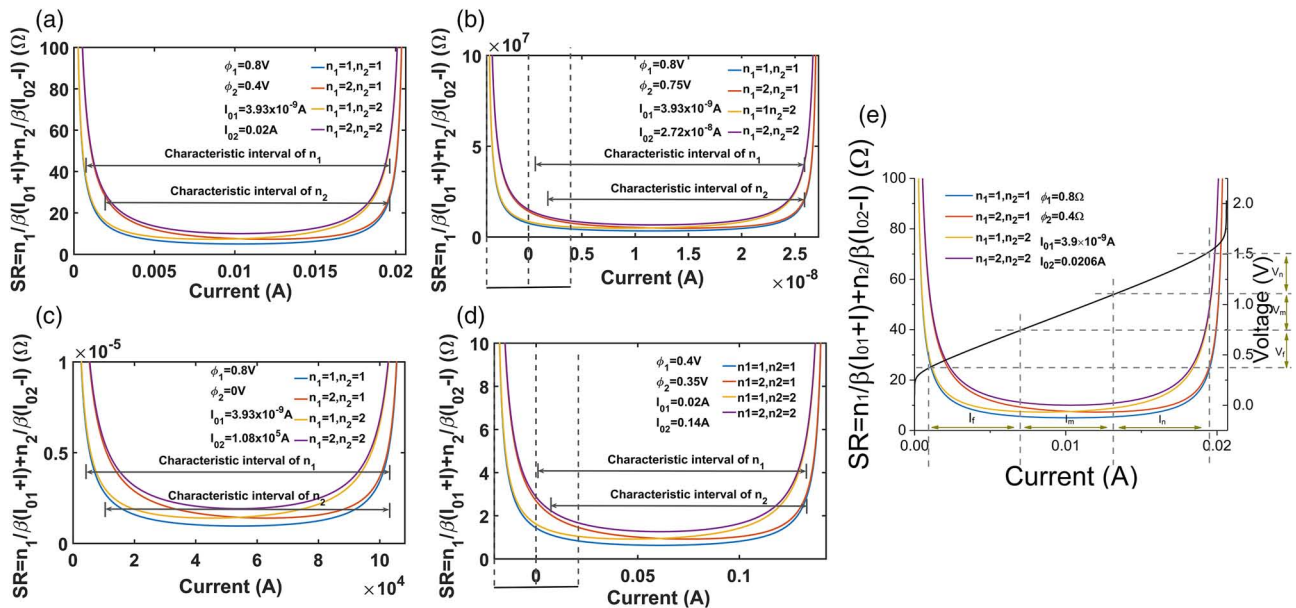


**Figure 4.** SR function under barrier heights of a)  $\phi_1 = 0.8$  V,  $\phi_2 = 0.4$  V, b)  $\phi_1 = 0.8$  V,  $\phi_2 = 0.75$  V, c)  $\phi_1 = 0.8$  V,  $\phi_2 = 0$  V, and d)  $\phi_1 = 0.4$  V,  $\phi_2 = 0.35$  V. e) Schematic diagram of interval selection for current and voltage under  $\phi_1 = 0.8$  V,  $\phi_2 = 0.4$  V.



Equation (3) can be rewritten as

$$V = \int_0^I \frac{dV}{dI} dI = \int_0^I \frac{n_1}{\beta(I_{01} + I)} dI + \int_0^I \frac{n_2}{\beta(I_{02} - I)} dI + \int_0^I R dI \quad (5)$$

Here the smaller saturation current is  $I_{01}$  and the larger one is  $I_{02}$ . According to the first part of Equation (5), on the right side, when the current is close to saturation current  $I_{01}$ , ideality factor  $n_1$  will be distinctively amplified and this is the start point of the characteristic interval of  $n_1$ . As the current increases, the distinction of  $n_1$  will not vanish but will accumulate till the current infinitely approaches  $I_{02}$ . Hence, the region  $[0.2I_{01}, 0.9I_{02}]$  is chosen as the characteristic interval of  $n_1$  in our calculation. And according to the second part of Equation (5), on the right side,  $n_2$  is the same as  $n_1$  and its characteristic interval becomes from  $0.1I_{02}$  to  $0.9I_{02}$ . However, according to the third part of Equation (5) on the right side, the start point of the characteristic interval of  $R$  only depends on the value of itself. If all saturation currents  $I_{01}$ ,  $I_{02}$  and  $R$  are small, the start point of the characteristic interval of  $R$  will not exist in a detectable interval, as shown in Figure 2i. In other words,  $R$  is unapproachable. According to the previous discussion, the selected characteristic intervals of ideality factors  $n_1$  and  $n_2$  in different barrier heights are shown in Figure 4a–d, respectively.

To reduce the accidental errors caused by a few points, three selected segments contained by the intersection of two characteristic intervals are used to solve the equations (see Figure 4e). As shown in Figure 4e, the current intervals  $I_f$ ,  $I_m$ , and  $I_n$  with corresponding voltage intervals  $V_f$ ,  $V_m$ , and  $V_n$  form three divided sections. The system of simultaneous equations (named System 1st) is expressed as

$$V_f = \frac{n_1}{\beta} \ln\left(\frac{I_f}{I_{01}} + 1\right) - \frac{n_2}{\beta} \ln\left(-\frac{I_f}{I_{02}} + 1\right) + RI_f \quad (6a)$$

$$V_m = \frac{n_1}{\beta} \ln\left(\frac{I_m}{I_{01}} + 1\right) - \frac{n_2}{\beta} \ln\left(-\frac{I_m}{I_{02}} + 1\right) + RI_m \quad (6b)$$

$$V_n = \frac{n_1}{\beta} \ln\left(\frac{I_n}{I_{01}} + 1\right) - \frac{n_2}{\beta} \ln\left(-\frac{I_n}{I_{02}} + 1\right) + RI_n \quad (6c)$$

where  $I_f$ ,  $I_m$ ,  $I_n$ ,  $V_f$ ,  $V_m$ , and  $V_n$  are the data from each interval. After cross-matching every data in the interval to establish simultaneous equations, there are  $f \times m \times n$  simultaneous equations. After obtaining parameter result groups, the frequency diagrams of those parameter groups are drawn to select the appropriate parameters. If the selected points are distributed evenly in the SR function, the results should accord with Gaussian distribution in theory. The expected value of the distribution is consequently chosen as the value of the parameter. But in practice, there might be one or several influence factors contributing a lot to the value of parameters, making the results not fit a Gaussian distribution. To fix this deviation, we need to select the mode of results as the value of parameters. If the curve is not complete enough to find out ideality factor  $n_2$  or series resistance  $R$ , which will result in an unreasonable frequency diagram, we fix  $n_2$  as unity to solve the equations system (named

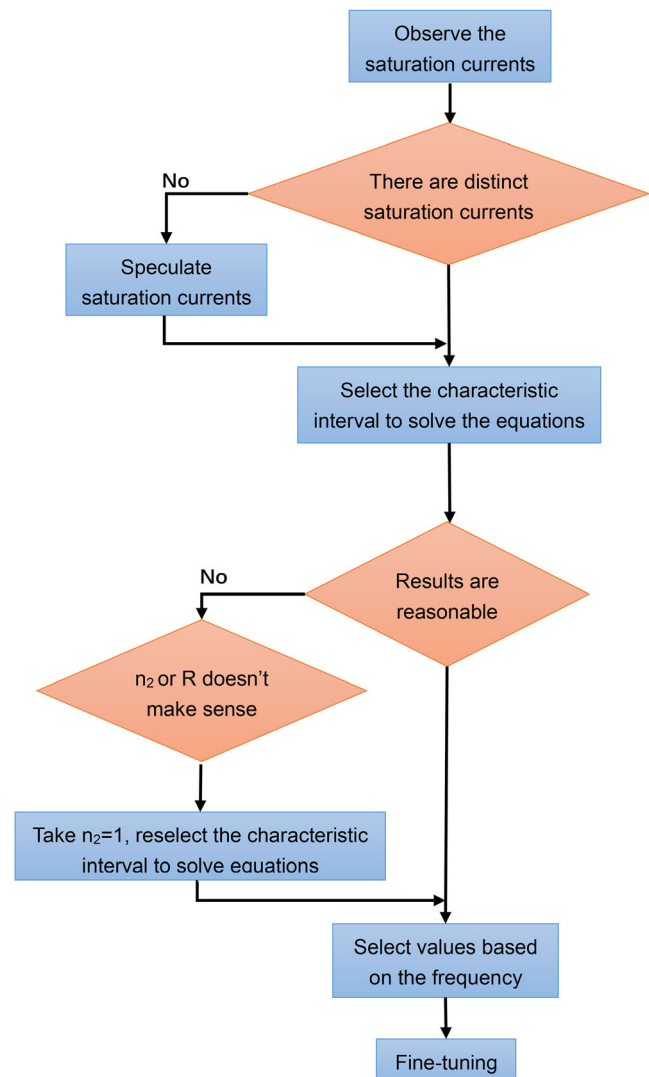


**Figure 5.** The flowchart of our extraction strategy.

System 2nd) with two unknowns. Without ideality factor  $n_2$ , the adopted data are from two segments, which are divided on average from the characteristic interval of  $n_1$ .

To verify the reliability of the calculated parameters, the final step is to draw the curve with the calculated parameters, compare it with the experimental curve, and then fine-tune them according to the rules summarized previously. A general flowchart of our strategy to approach the parameters is shown in Figure 5.

## 5. Results and Discussion

To verify the accuracy of the aforementioned method and as a demonstration, this method is used on several representative curves generated according to Equation (3) at room temperature. Following the flowchart (Figure 5), we first manually take points from the generated standard curve, as shown in part (a) of Figure S1–S6, Supporting Information. After that, the saturation currents are obtained from the end point of the picked curves,

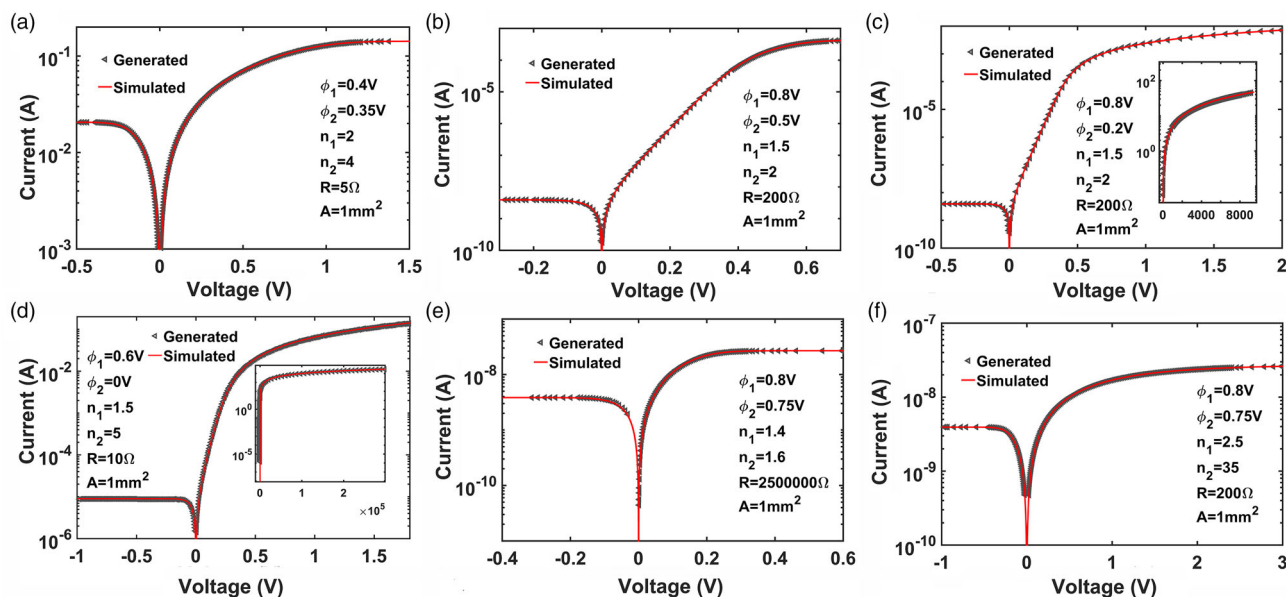


**Figure 6.** Standard curves generated comparing with our fitting curves. a) In both barrier heights are low and the difference is small ( $\phi_1 = 0.4$  V and  $\phi_2 = 0.35$  V). b,c) The same series resistance ( $R = 200 \Omega$ ) in two different barrier heights. d) The extreme condition when  $\phi_1 = 0.6$  V and  $\phi_2 = 0$  V. e,f) The same barrier heights ( $\phi_1 = 0.8$  V and  $\phi_2 = 0.75$  V) in two different series resistances.

and the SR function (part (b) of Figure S1–S6, Supporting Information) is drawn to select the characteristic interval. After the calculation, by substituting data into Equation (6a)–(6c), the frequency diagrams of the two ideality factors and series resistance are drawn (see S1–S6, Supporting Information). One can see that the diagrams of Figure S1, S2, S5, and S6, Supporting Information, are reasonable, and the parameter values are adopted to fitting curves (part (f) of Figure S1, S2, S5, and S6, Supporting Information). However, in Figure S6e, Supporting Information, the series resistance  $R$  is not large enough to be identified, compared with Figure S5e, Supporting Information. In addition, in Figure S3d, Supporting Information, the barrier heights are too small to identify the ideality factor  $n_2$  from the generated curve. Hence, we fix  $n_2$  as 1 to resolve System 2nd (as shown in Figure S3f, S3g, S4c, and S4d, Supporting Information). Furthermore, the value of  $n_2$  is varied to show its validity in Figure S4f, Supporting Information, from which one can see  $n_2$  is indistinguishable within a reasonable range of values. In other words, we can assume that  $n_2$  is any value in a range much smaller than  $10^5$  and this does not affect the solution; meanwhile,  $n_2$  itself has lost physical meaning and

become a technical parameter. For simplicity,  $n_2$  can always be set as 1. What needs to be state here is that ideality factor  $n_2$  in Figure S4 and S6, Supporting Information, is too large to be described completely by thermionic emission, which means  $n_2$  in these figures are also just technical parameters. But from  $n_2$  in Figure S4, Supporting Information, one can see that  $n_2$  cannot be extracted even if  $n_2$  is as large as 5, and in Figure S5 and S6, Supporting Information, one can see that  $n_2$  is accessible no matter whether  $n_2$  itself is small or large when the barrier of this diode allows it. As a result, all simulations are in Figure 6, and the parameters extracted are compared with standard parameters in Table 1. More details are shown in the Supporting Information (Figure S1–S6). By comparing Figure 6 and Table 1, it can be seen that the parameters obtained by our method is very consistent with the original parameters, which indirectly proves that this is an effective extraction method.

Moreover, to further verify the feasibility of our method, four reported current–voltage curves from previous articles were chosen for the extraction process and the results are shown in Figure 7 and Table 2–6.<sup>[43–46]</sup> In those fitting curves, literature fitting only presented us with one ideality factor or with

**Table 1.** Standard parameters and extracted parameters in Figure 6.

	Figure 6a		Figure 6b		Figure 6c		Figure 6d		Figure 6e		Figure 6f	
	Generated	Our result	Generated	Our result	Generated	Our result	Generated	Our result	Generated	Our result	Generated	Our result
$\phi_1$ [V]	0.4	0.4001	0.8	0.8001	0.8	0.8001	0.6	0.6004	0.8	0.8006	0.8	0.8
$\phi_2$ [V]	0.35	0.3501	0.5	0.5001	0.2	0.2001	0	0.0013	0.75	0.7503	0.75	0.7501
$n_1$	2	2	1.5	1.497	1.5	1.49	1.5	1.52	1.4	1.52	2.5	2.6
$n_2$	4	4	2	1.87	2	–	5	–	1.6	1.7	35	35
$R[\Omega]$	5	5	200	210	200	201	10	10	2 500 000	2 200 000	200	–

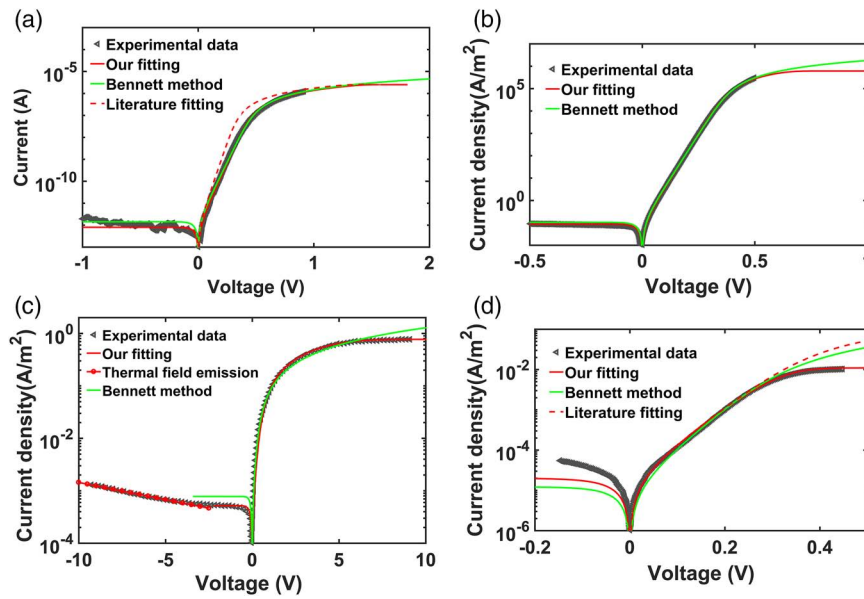


**Figure 7.** Previously reported experimental curves with several simulations. a) Experimental curve comparing with our fitting, Bennett fitting and literature fitting. b) Experimental curve with our fitting and Bennett method. c) Experimental curve with our fitting, Bennett method and thermal field emission fitting. d) Experimental curve with our fitting, Bennett fitting and literature fitting.

**Table 2.** Parameters of all curves in Figure 7a.

	$I_{01}$ [A]	$I_{02}$ [A]	$n_1$	$n_2$	$R$ [ $\Omega$ ]
Literature fitting	–	–	1.09	–	–
Our fitting before fine-tuning	$6.5 \times 10^{-13}$	$2.51 \times 10^{-6}$	1.36	1	$3.2 \times 10^5$
Our fitting	$8 \times 10^{-13}$	$2.51 \times 10^{-6}$	1.45	1	$3.2 \times 10^5$
Bennett method	$1.43 \times 10^{-12}$	–	1.55	–	$3.04 \times 10^5$

**Table 3.** Parameters of all curves in Figure 7b.

	$\phi_1$ [V]	$\phi_2$ [V]	$n_1$	$n_2$	RA [ $\Omega$ m <sup>2</sup> ]
Our fitting before fine-tuning	0.7240	0.3122	1.01	1	$3.5 \times 10^{-7}$
Our fitting	0.7196	0.3122	1.04	1	$3 \times 10^{-7}$
Bennett method	0.7148	–	1.33	–	$1.2 \times 10^{-6}$

**Table 4.** Parameters of all curves in Figure 7c.

	$\phi_1$ [V]	$\phi_2$ [V]	$n_1$	$n_2$	RA [ $\Omega$ m <sup>2</sup> ]
Our fitting	0.8523	0.6635	4.43	34	4
Bennett method	0.8418	–	3.67	–	7.25

**Table 5.** Reverse bias fitting in Figure 7c.

	$a$	$b$	$C$
Reverse bias fitting	$3.18 \times 10^{-6}$	–0.15	$1 \times 10^4$

one barrier height (see Table 2 and 6), while the rest of the parameters that Equation (3) needs are from our result. In addition, the curves fitted by the Bennett method in Figure 7 all use the single diode model, which conforms to Equation (1). The adopted interval for Bennett's calculation is the identical region found by Nouchi.<sup>[21,39]</sup> Therefore, the green curves always go up exponentially under a large forward bias. As a part of the extraction procedure, our fitting parameters before fine-tuning are also shown in Table 2, 3, and 6. Furthermore, the unsaturated current under reverse bias in Figure 7c was fitted using the least square method by thermionic field emission mechanism under reverse bias (see Figure S9, Supporting Information). In those extracted parameters, the barrier heights in Figure 7a can be obtained from Equation (2) theoretically (not given here due to the lack of area  $A$  in Equation (2)) and the barrier heights in other figures were calculated using the standard Richardson constant ( $A^{**} = 1.2 \times 10^6 \text{ A m}^{-2} \text{ K}^{-2}$ ) (given experimental data are current density–voltage, the area  $A$  in Equation (2) is unnecessary to calculate barrier height). It can be extrapolated that barrier  $\phi_2$  in Table 2 and 3 are both not large enough to make  $n_2$  distinguishable; hence, it is more reasonable to fix  $n_2$  as unity. However, in the case of Table 6 the characteristic intervals of  $n_2$  and  $R$  overlap and the result becomes doubtful, because the fitting curve of

**Table 6.** Parameters of all curves in figure 7d.

	$\phi_1$ [V]	$\phi_2$ [V]	$n_1$	$n_2$	RA [ $\Omega$ m <sup>2</sup> ]
Literature fitting	0.9044	–	1.9	–	–
Our fitting before fine-tuning	0.9365	0.7734	1.97	1	1.5
Our fitting	0.9365	0.7734	1.9	1	1.5
Bennett method	0.9493	–	1.33	–	4.16

$n_2 = 1$  and  $RA = 1.5 \Omega \text{ m}^2$  are almost overlapped with the curve of  $n_2 = 1.5$  and  $RA = 0 \Omega \text{ m}^2$  (see Figure S10p, Supporting Information). From Figure 7 and Table 2–5, one can see the fitting curves are highly compatible with experimental curves, which indicates our extraction method is effective. More details are shown in the Supporting Information (Figure S7–S10).

## 6. Conclusions

In summary, the current–voltage characteristics of MSM diodes under the impact of various parameters were investigated. From the investigation of characteristic parameters of two back-to-back connected Schottky contacts, we present two empirical conclusions: 1) the ideality factor of one Schottky diode becomes distinguishable in the detectable coordinate scale only if the barrier height of this Schottky diode is high enough. 2) Series resistance is recognized only when the series resistance is big enough that it drives the current–voltage curves already in reverse direction of the studied diodes, either the first diode or the second one.

A method via solving equations during the characteristic interval was proposed to extract the parameters from the current–voltage curve of two back-to-back connected Schottky contacts. The Schottky parameters of the MSM interface could be calculated by the following procedure: 1) saturation currents must be attainable or conjecturable from the current–voltage curve and barrier heights can be derived. If two saturation currents are hidden by an incomplete curve or some other physical mechanism, try to treat the measured current under bias of  $-0.1 \text{ V}$  as reverse saturation current, and the extrapolation of forward saturation current can be seen in the Supporting Information. 2) Plot the SR function to select appropriate intervals of current and voltage. 3) Solve System 1st established by cross-matching each point in the intervals of current and voltage. 4) Choose values from the frequency diagrams of parameters. If the frequency diagrams are not adoptable, reselect the intervals to calculate System 2nd. 5) Draw the curve using calculated results and compare with original curve. If there is any deviation, fine-tune the curve according to the following experiences: Ideality factor  $n_1$  determines the slope of the linear part of the curve under logarithmic coordinates, and series resistance  $R$  determines when the linear part bends down to form an exponential curve. Comparing standard curves with our simulations, it can be seen that this method is highly feasible. Moreover, this method is verified through the extraction of experimental curves, and the curves from extracted parameters are compatible with the experimental curves.

## Supporting Information

Supporting Information is available from the Wiley Online Library or from the author.

## Acknowledgements

This work was partially supported by the China Postdoctoral Science Foundation (Grant No. 2018M643443), National Natural Science Foundation of China (Grant No. 51802032 and 11675029), Science and

Technology Research Fund of Sichuan Province (Grant No. 2017Y0320 and 2018Y0513), and National undergraduate innovation and entrepreneurship training program (Grant No. 201810621051 and S201910621092). This article was amended on April 24, 2020 to correct figure 6.

## Conflict of Interest

The authors declare no conflict of interest.

## Keywords

barrier height, ideality factor, Schottky devices, series resistance, thermionic emission theory

Received: December 10, 2019

Revised: February 2, 2020

Published online: February 26, 2020

- [1] W. Tian, H. Sun, L. Chen, P. Wangyang, X. Chen, J. Xiong, L. Li, *InfoMat.* **2019**, 1, 140.
- [2] C. Yan, C. Gong, P. Wangyang, J. Chu, K. Hu, C. Li, X. Wang, X. Du, T. Zhai, Y. Li, J. Xiong, *Adv. Funct. Mater.* **2018**, 28, 1803305.
- [3] C. Gong, K. Hu, X. Wang, P. Wangyang, C. Yan, J. Chu, M. Liao, L. Dai, T. Zhai, C. Wang, L. Li, J. Xiong, *Adv. Funct. Mater.* **2018**, 28, 1706559.
- [4] J. Chu, F. Wang, L. Yin, L. Lei, C. Yan, F. Wang, Y. Wen, Z. Wang, C. Jiang, L. Feng, J. Xiong, Y. Li, J. He, *Adv. Funct. Mater.* **2017**, 27, 1701342.
- [5] J. Wang, J. Han, X. Chen, X. Wang, *InfoMater.* **2019**, 1, 33.
- [6] G. Rao, X. Wang, Y. Wang, P. Wangyang, C. Yan, J. Chu, L. Xue, C. Gong, J. Huang, J. Xiong, Y. Li, *InfoMater.* **2019**, 1, 272.
- [7] A. Sellai, Z. Ouennoughi, *Int. J. Mod. Phys. C* **2005**, 16, 1043.
- [8] E. H. Rhoderick, E. Rhoderick, *Metal-Semiconductor Contacts*, Clarendon Press, Oxford, UK **1978**.
- [9] S. M. Sze, K. K. Ng, *Physics of Semiconductor Devices*, Wiley, Hoboken, NJ **2006**.
- [10] K. Akkiliç, M. E. Aydin, A. Türüt, *Phys. Scr.* **2004**, 70, 364.
- [11] M. E. Aydin, K. Akkiliç, T. Kiliçoğlu, *Appl. Surf. Sci.* **2006**, 253, 1304.
- [12] G. Liang, T. Cui, K. Varahramyan, *Solid-State Electron.* **2003**, 47, 691.
- [13] H. Norde, *J. Appl. Phys.* **1979**, 50, 5052.
- [14] K. Sato, Y. Yasumura, *J. Appl. Phys.* **1985**, 58, 3655.
- [15] C. D. Lien, F. C. T. So, M. A. Nicolet, *IEEE Trans. Electron Devices* **1984**, 31, 1502.
- [16] S. K. Cheung, N. W. Cheung, *Appl. Phys. Lett.* **1986**, 49, 85.
- [17] J. H. Werner, *Appl. Phys. A* **1988**, 47, 291.
- [18] D. Donoval, M. Barus, M. Zdimal, *Solid-State Electron.* **1991**, 34, 1365.
- [19] V. Aubry, F. Meyer, *J. Appl. Phys.* **1994**, 76, 7973.
- [20] J. Osvald, E. Dobročka, *Semicond. Sci. Technol.* **1996**, 11, 1198.
- [21] R. J. Bennett, *IEEE Trans. Electron Devices* **1987**, 34, 935.
- [22] V. Mikhelashvili, G. Eisenstein, R. Uzdin, *Solid-State Electron.* **2001**, 45, 143.
- [23] A. Ferhat-Hamida, Z. Ouennoughi, A. Hoffmann, R. Weiss, *Solid-State Electron.* **2002**, 46, 615.
- [24] D. Gromov, V. Pugachevich, *Appl. Phys. A* **1994**, 59, 331.
- [25] R. M. Cibils, R. H. Buitrago, *J. Appl. Phys.* **1985**, 58, 1075.
- [26] K. E. Bohlin, *J. Appl. Phys.* **1986**, 60, 1223.
- [27] A. Ortiz-Conde, Y. Ma, J. Thomson, E. Santos, J. J. Liou, F. J. G. Sánchez, M. Lei, J. Finol, P. Layman, *Solid-State Electron.* **1999**, 43, 845.



- [28] E. K. Evangelou, L. Papadimitriou, C. A. Dimitriades, G. E. Giakoumakis, *Solid-State Electron.* **1993**, 36, 1633.
- [29] A. Ortiz-Conde, F. J. G. Sanchez, *Solid-State Electron.* **2005**, 49, 465.
- [30] A. Sellami, M. Zagrouba, M. Bouaïcha, B. Bessaïs, *Meas. Sci. Technol.* **2007**, 18, 1472.
- [31] Y. Li, *Microelectron. Eng.* **2007**, 84, 260.
- [32] F. Li, S. P. Mudanai, Y.-Y. Fan, W. Zhao, L. F. Register, S. K. Banerjee, in *Proc. 15th Biennial University/Government/Industry Microelectronics Symp. (Cat. No. 03CH37488)*, Boise, USA **2003**.
- [33] M. Thomas, C. Pacha, K. Goser, in *Proc. International Conf. on Computational Intelligence*, Dortmund, Germany **1999**.
- [34] K. Wang, M. Ye, *Solid-State Electron.* **2009**, 53, 234.
- [35] B. Lakehal, A. Dendouga, *J. Nano- Electron. Phys.* **2018**, 10, 06046-1-06046-4.
- [36] A. J. Chiquito, C. A. Amorim, O. M. Berengue, L. S. Araujo, E. P. Bernardo, E. R. Leite, *J. Phys. Condens Matter* **2012**, 24, 225303.
- [37] M. Ahmetoglu, S. K. Akay, *Curr. Appl. Phys.* **2010**, 10, 652.
- [38] V. Mikhelashvili, R. Padmanabhan, G. Eisenstein, *J. Appl. Phys.* **2017**, 122, 034503.
- [39] R. Nouchi, *J. Appl. Phys.* **2014**, 116, 184505.
- [40] E. H. Rhoderick, R. H. Williams, *Metal-Semiconductor Contacts*, 2nd ed., Clarendon Press, Oxford, UK **1988**.
- [41] J. Osvald, *Phys. Status Solidi A* **2015**, 212, 2754.
- [42] F. Hernandez-Ramirez, A. Tarancon, O. Casals, E. Pellicer, J. Rodriguez, A. Romano-Rodriguez, J. R. Morante, S. Barth, S. Mathur, *Phys. Rev. B* **2007**, 76, 085429.
- [43] Y. Liu, J. Guo, E. Zhu, L. Liao, S. J. Lee, M. Ding, I. Shakir, V. Gambin, Y. Huang, X. Duan, *Nature* **2018**, 557, 696.
- [44] F. Guo, B. Yang, Y. Yuan, Z. Xiao, Q. Dong, Y. Bi, J. Huang, *Nat. Nanotechnol.* **2012**, 7, 798.
- [45] G. Li, Z. Li, J. Chen, X. Chen, S. Qiao, S. Wang, Y. Xu, Y. Mai, *J. Alloys Compd.* **2018**, 737, 67.
- [46] B. C. Min, K. Motohashi, C. Lodder, R. Jansen, *Nat. Mater.* **2006**, 5, 817.